Available online at www.sciencedirect.com
SCIENCE DIRECT
Physica D 215 (2006) 80–98
PHYSICA D
www.elsevier.com/locate/physd

Grain boundary motion arising from the gradient flow of the Aviles–Giga functional

K.B. Glasner*

Department of Mathematics, University of Arizona, 617 N Santa Rita, Tucson, AZ 85721, United States

Received 27 June 2005; received in revised form 17 January 2006; accepted 18 January 2006
Available online 3 March 2006
Communicated by J. Lega

Abstract

This paper considers the singular limit of the equation $\Theta_t = -\epsilon\Delta^2\Theta + \epsilon^{-1}\nabla\cdot([|\nabla\Theta|^2 - 1]\nabla\Theta)$. Grain boundaries (limiting discontinuities in $\nabla\Theta$) form networks that coarsen over time. A matched asymptotic analysis is used to derive a free boundary problem consisting of curve motion coupled along hyperbolic characteristics and junction conditions. An intermediate boundary layer near extrema junctions is discovered, along with the relevant nonlocal junction conditions. The limiting dynamics can be viewed in the context of a gradient flow of the sharp interface energy on an attracting manifold. Dynamic scaling of the long-time coarsening process can be explained by dimensional analysis of the reduced problem.

Keywords: Grain boundaries; Matched asymptotic expansion; Gradient flows

1. Introduction

This paper explores the dynamics of the equation

$$\Theta_t = -\epsilon\Delta^2\Theta + \epsilon^{-1}\nabla\cdot(B\nabla\Theta) \quad B = |\nabla\Theta|^2 - 1 \tag{1}$$

in the singular limit $\epsilon \to 0$. In this limit, it is well understood that $\nabla\Theta$ becomes discontinuous along curves known as phase grain boundaries. These defects connect at junctions to form networks which evolve and gradually coarsen.

Eq. (1) has the variational structure $\Theta_t = -\delta E$ where the energy is

$$E = \int \frac{\epsilon}{2}(\Delta\Theta)^2 + \frac{1}{4\epsilon}(1 - |\nabla\Theta|^2)^2 \mathrm{d}x. \tag{2}$$

This functional was first proposed by Aviles and Giga [2] to model smectic liquid crystals, and it has also appeared in the study of thin-film blistering [21]. Similar free energies are used extensively in theories of magnetic domains (e.g. [14]).

The gradient flow (1) has also appeared in various contexts. In the pattern formation literature, it is known as the regularized Cross–Newell phase diffusion equation [5,7], which derives from the study of roll patterns under a modulation theory ansatz. Eq. (1) and its variants have also been used to study the evolution of epitaxial thin films driven by adatom diffusion [26].

In the limit of small ϵ, it is understood that energy concentrates along grain boundary curves [1,6] in the following sense. If $E_\epsilon(\Theta_\epsilon)$ is a bounded sequence, then the limit of $\nabla\Theta_\epsilon$ is compact in L^2 and its limit satisfies the eikonal equation $|\nabla\Theta|^2 = 1$ almost everywhere. In the time-dependent case, we might expect that there is a rapid but transient period over which energy relaxes to

* Tel.: +1 520 621 4764.
E-mail address: kglasner@math.arizona.edu.

0167-2789/$ - see front matter
doi:10.1016/j.physd.2006.01.013

an $\mathcal{O}(1)$ value. From that point onward, the eikonal equation is approximately satisfied everywhere except along grain boundary curves where energy concentrates. As a consequence, the limiting dynamics must be driven simply by information on the curves themselves.

A principal aim of this paper is to extract the motions of grain boundary curves from the partial differential equation using matched asymptotic expansions. We find that the dynamics of the grain boundaries arise from curvature of the interfaces and variation in the "line energy" (associated with how sharply rolls meet at the grain boundaries) along each grain boundary. Conditions at junctions where grain boundaries meet are also derived. It is discovered that some junctions have a secondary boundary layer that leads to a nonlocal type of junction condition. The end result is a complicated but tractable free boundary problem for the grain boundary curves. This evolution is shown to be the gradient flow of the sharp interface energy on an appropriate manifold.

The overall nature of the dynamics falls into the category of energy driven coarsening processes (e.g. [9,13,16,18]), characterized by growth of the typical length scale $L(t) \sim t^{\alpha}$ as $t \to \infty$, where α is the scaling exponent. Rost and Krug [25] consider dynamic scaling of the characteristic length as a function of time for a family of related equations. Moldovan and Golubovic [19] give theoretical and numerical arguments for scaling behavior. Ortiz et al. [22] predict scaling exponents using an explicit construction based on the sharp interface energy. Rigorous bounds on the rate of energy decrease were obtained by Kohn and Yan [17]. All these authors predict a scaling exponent of $\alpha = 1/3$.

The reasons for coarsening are energetic: both the original energy (2) and its singular limit (85) penalize large spatial gradients associated with fine scale structures. The gradient nature of the dynamics means that solutions will therefore typically seek out lower energy states with larger features. Of course, the variational structure of the problem does not guarantee coarsening: arbitrary initial data may lie on a stable manifold of a hyperbolic fixed point, and the system can get stuck.

As with phase-separation processes that lead to motion by curvature or surface diffusion [9,16], the scale invariance of the system leads to a natural conjecture about the scaling exponent. Eq. (1) does not exactly possess the necessary scale invariance, but we find that the sharp interface grain boundary dynamics does (see Eqs. (51), (53) and (54)). In particular, if L is a characteristic length, then rescaling lengths by L and time by L^2 leads to exactly the same system. In other words, everything should evolve at a rate proportional to L^{-2}, including L itself. This leads to $\mathrm{d}L/\mathrm{d}t \sim L^{-2}$ which integrates to the desired conclusion $L \sim t^{1/3}$.

2. Numerical observations

To inspire the subsequent analysis, a numerical simulation of (1) was conducted using a highly stable split-step method for variational dynamics [8], where the boundary conditions are reflecting (zero first and third normal derivatives). Fig. 1 shows the energy density of the solution (the integrand of (2)) at several different times. Concentration of the energy into a network of curves is obvious. Individual curves within this network migrate over time, leading to coalescence or annihilation of grain boundaries, and the merging of junctions. Note that the energy density varies in intensity (gray vs. white) along each grain boundary, reflecting the fact that roll patterns meet at different angles. In some cases, the angle between them become so mild that the grain boundary nearly vanishes and is nearly indistinguishable from the bulk (this is very evident in the final panel of Fig. 1). This raises the question of whether or not phase grain boundaries may terminate in the bulk instead of at junction points. We do not consider this possibility here, but such structures cannot be ruled out when Dirichlet boundary conditions are imposed [7].

Fig. 2 shows a typical situation after some coarsening has occurred. The energy density is plotted along with contours of Θ. Two different types of junctions are observed. Saddle points (A) are where four junctions meet, ostensibly at right angles. Extrema junctions (B) are minima or maxima of Θ, and many connect several grain boundaries. We also plotted a few streamlines of $\nabla\Theta$ (which are characteristics of the eikonal equation, see the next section) which emanate from extrema junctions. These will play a crucial role in developing a complete description of junctions (Section 4).

3. The sharp interface limit of grain boundary motion

The fourth order term in (1) is a singular perturbation which can be treated by a fairly standard (albeit lengthy) matched asymptotic analysis. The principal assumption is that in the limit $\epsilon \to 0$, the solution remains smooth on a set of open subdomains $\{\Omega_n\}$ we shall call *grains*. Furthermore, it is supposed that the complement of the union of all grains is composed of a set of smooth curves (grain boundaries) whose endpoints meet at a set of junctions (see Fig. 3). Expansions are sought both away from grain boundaries and in a rescaled region around each boundary. Junctions will be dealt with in a subsequent section.

3.1. Solutions away from grain boundaries

Within each grain Ω_n and away from the grain boundary we anticipate that an "outer" solution can be found for Eq. (1) by expanding in a regular series $\Theta = \Theta^{(0)} + \epsilon\Theta^{(1)} + \epsilon^2\Theta^{(2)} + \ldots$. The leading order solution will simply be called Θ to avoid excessive notation. At leading order we obtain

$$\nabla \cdot ([|\nabla\Theta|^2 - 1]\nabla\Theta) = 0. \tag{3}$$

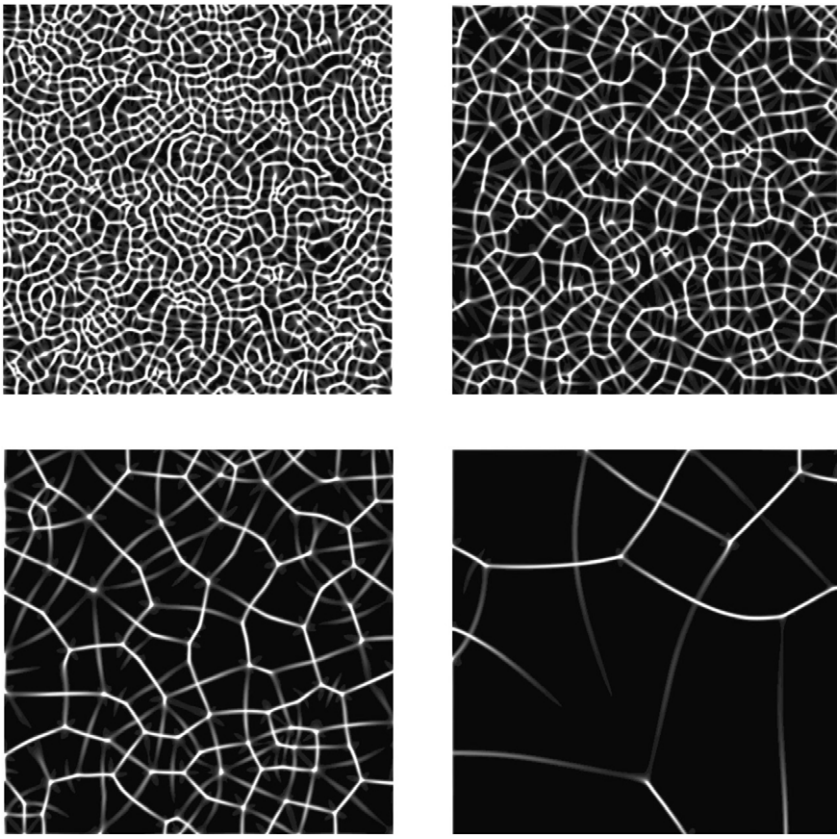

Fig. 1. Numerical simulation of (1) at several times, showing the energy density. The initial data was random, $\epsilon = .4$, and the numerical grid was 1024^2 with size $\Delta x = 0.2$.

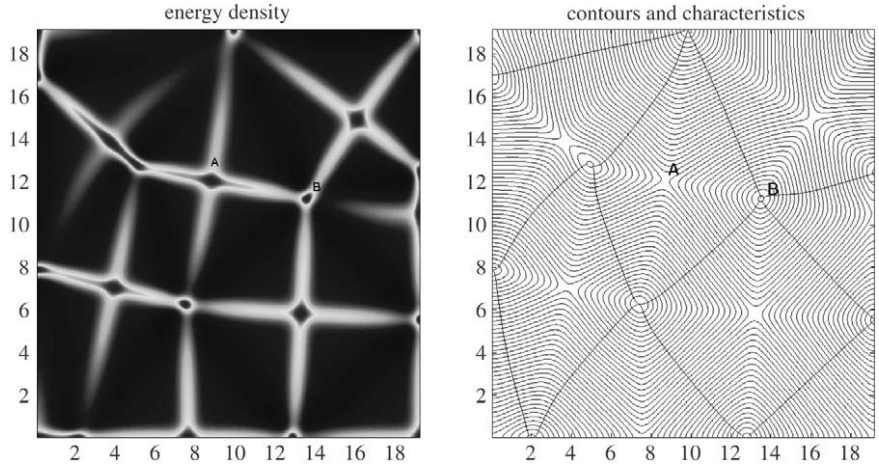

Fig. 2. Numerical simulation (256×256, $\epsilon = .2$, $\Delta x = .075$) showing a typical grain boundary network. On the left, the energy density is plotted. The corresponding contours of Θ are shown on the right, together with a few select "streamlines" (i.e. characteristics) of $\nabla\Theta$. There are two junction types represented: (A) a saddle junction, (B) an extrema junction.

We are interested only in smooth solutions to this equation that are minimizers of the associated variational problem

$$\min \int_{\Omega_n} (1 - |\nabla\Theta|^2)^2 \mathrm{d}x. \tag{4}$$

In other words, the leading order problem is the eikonal equation

$$|\nabla\Theta|^2 = 1. \tag{5}$$

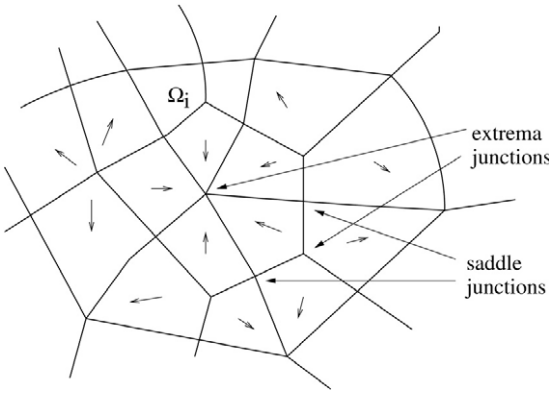

Fig. 3. Schematic of a grain boundary network, consisting of grains Ω_i, and grain boundary curves that meet at junctions. The small arrows show the direction of $\nabla\Theta$.

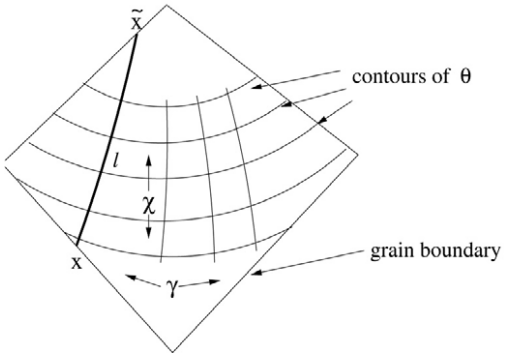

Fig. 4. Caricature of a single grain, showing level sets of the leading order solution $\Theta \equiv \chi$. Orthogonal to these are level sets of the coordinate γ and the characteristic curves $\ell(\gamma)$.

We now introduce the coordinate system (χ, γ) (see Fig. 4) in which $\chi \equiv \Theta$ and γ is chosen to be the arclength along some arbitrary contour $\chi = \Theta^*$. Observe that the γ contours are the characteristic curves of the hyperbolic eikonal equation which will play an important role in transferring information between their endpoints which live on grain boundaries. The metric in this orthogonal coordinate system is

$$\mathrm{d}s^2 = \mathrm{d}\chi^2 + G^{-2}\mathrm{d}\gamma^2, \quad G_\chi = -K(\chi, \gamma)G \tag{6}$$

where $K = \Delta\Theta$ is the curvature of the level sets of Θ. Integration gives the explicit formula

$$G(\chi, \gamma) = \exp\left(-\int_{\Theta^*}^{\chi} K(\chi', \gamma)\mathrm{d}\chi'\right). \tag{7}$$

The next order in the expansion reads

$$\Theta_t = 2\nabla\cdot\left([\nabla\Theta\cdot\nabla\Theta^{(1)}]\nabla\Theta\right) \equiv 2\mathcal{L}\Theta^{(1)}. \tag{8}$$

In (χ, γ) coordinates this simplifies to

$$\Theta_t = 2(\Theta^{(1)}_{\chi\chi} + K\Theta^{(1)}_\chi), \tag{9}$$

where the time derivative is still with respect to a non-moving coordinate system. Using (6)b, the linear operator in Eq. (9) can be written

$$\mathcal{L} = \frac{\partial^2}{\partial\chi^2} - G_\chi G^{-1}\frac{\partial}{\partial\chi}. \tag{10}$$

This operator is self-adjoint with respect to the weighted inner product

$$\langle\psi_1, \psi_2\rangle = \int_{\Omega_i} \psi_1\psi_2 G^{-1}(\chi, \gamma)\mathrm{d}\chi\,\mathrm{d}\gamma \tag{11}$$

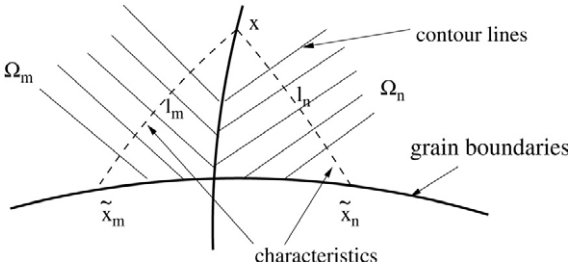

Fig. 5. Dynamics at a point x on the grain boundary depend on information at the three boundary points $x, \tilde{x}_n$ and $\tilde{x}_m$ which are connected by the characteristic curves ℓ of the leading order solution.

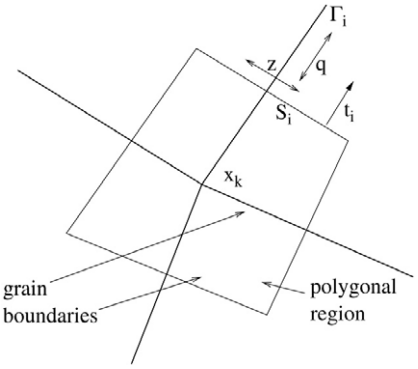

Fig. 6. Diagram of the polygonal region that encloses the grain boundary junction. For each side S_i, a coordinate system (z, q) is used which coincides with the one used for the grain boundary Γ_i.

which is just the usual L^2 inner product written in (χ, γ) coordinates. The nullspace of $\mathcal{L}$ is easily found by integration with respect to χ, and is spanned by $C_1(\gamma)G_2,\ C_2(\gamma)$ where

$$G_2 = \int G(\chi, \gamma)\mathrm{d}\chi \tag{12}$$

and C_1, C_2 are arbitrary functions of γ.

Solvability conditions are implied by an inner product of (9) with functions in the nullspace. Note that by differentiating (5) with respect to time gives

$$\nabla\Theta \cdot \nabla\Theta_t = \frac{\partial\Theta_t}{\partial\chi} = 0, \tag{13}$$

which implies that Θ_t is a function of γ alone. The first solvability condition is given by setting $C_1 = 0$ and taking inner products. It suffices to set C_2 equal to the delta function $\delta(\gamma)$ for each γ, so that the two dimensional inner product reduces to a one dimensional integral along each characteristic curve $\ell(\gamma) = \{(\chi, \gamma) \in \Omega_i\}$:

$$\begin{aligned}\int_\ell \Theta_t G^{-1}\mathrm{d}\chi &= 2\int_\ell \Theta^{(1)}_{\chi\chi}G^{-1} - G_\chi G^{-2}\Theta^{(1)}_\chi \mathrm{d}\chi \\ &= 2[\Theta^{(1)}_\chi G^{-1}]^{\tilde{x}(\gamma)}_{x(\gamma)}.\end{aligned} \tag{14}$$

Hereafter, the notation $x(\gamma), \tilde{x}(\gamma)$ will denote endpoints of each curve $\ell(\gamma)$, oriented so that $\Theta(x) < \Theta(\tilde{x})$ (see Fig. 5). Using the fact that $\chi \equiv \Theta$, in the original coordinates the dynamics of the leading order solution on each curve $\ell(\gamma)$ are

$$|\ell|\Theta_t = 2[\nabla\Theta \cdot \nabla\Theta^{(1)}G^{-1}]^{\tilde{x}(\gamma)}_{x(\gamma)}, \quad |\ell| = \int_\ell G^{-1}\mathrm{d}\chi. \tag{15}$$

The second solvability condition is obtained similarly by taking an inner product of (9) with $\delta(\gamma)G_2$. It provides boundary conditions for solving the next order problem, but is not needed for what follows.

3.2. Grain boundary solutions

The "inner" solution at the grain boundaries relies on the use of a moving fitted orthogonal coordinate system (r, s) that has been used in numerous other studies (e.g. [4,24]). The coordinate r designates the signed distance to the boundary and s the

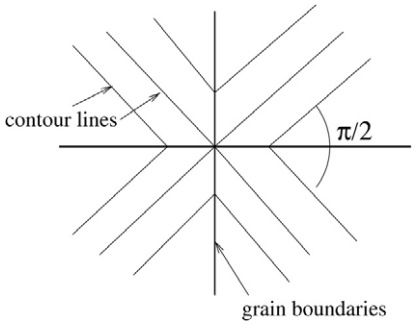

Fig. 7. Observed configuration of saddle junctions. Grain boundaries and contours all meet at an angle of $\pi/2$.

distance along it, and the orientation is chosen so that $r > 0$ in Ω_i. The transverse coordinate is rescaled by setting $z = r/\epsilon$ so that derivatives rescale as $\partial/\partial r = \epsilon^{-1}\partial/\partial z$. To differentiate from the outer solution, lowercase notation $\Theta = \theta(z, s, t)$ will be employed. To organize the calculation, we introduce the intermediate quantities

$$B = \epsilon^2(|\nabla\Theta|^2 - 1) = \theta_z^2 + \epsilon^2|\nabla s|^2\theta_s^2 - \epsilon^2, \tag{16}$$

$$M = -\epsilon^2\Delta\Theta = -\theta_{zz} - \epsilon(\Delta r)\theta_z - \epsilon^2|\nabla s|^2\theta_{ss} - \epsilon^2(\Delta s)\theta_s. \tag{17}$$

In the moving coordinate system, Eq. (1) takes the form

$$\begin{aligned}\theta_t + \epsilon^{-1}\theta_z r_t + \theta_s s_t = {} & \epsilon^{-3}M_{zz} + \epsilon^{-2}(\Delta r)M_z + \epsilon^{-1}|\nabla s|^2 M_{ss} + \epsilon^{-1}(\Delta s)M_s \\ & + \epsilon^{-5}(B\theta_z)_z + \epsilon^{-4}B(\Delta r)\theta_z + \epsilon^{-3}B(\Delta s)\theta_s + \epsilon^{-3}|\nabla s|^2(B\theta_s)_s.\end{aligned} \tag{18}$$

All quantities θ, B, M are expanded in powers of ϵ. In addition, the coordinate derivatives expand as

$$\Delta r = -\kappa + \mathcal{O}(\epsilon) \tag{19}$$

$$|\nabla s|^2 = 1 + 2\kappa\epsilon z + \mathcal{O}(\epsilon^2) \tag{20}$$

$$\Delta s = \mathcal{O}(\epsilon), \tag{21}$$

where κ is the curvature of the boundary, oriented so that if $r > 0$ is the interior of a convex region, $\kappa > 0$. Terms with like powers of ϵ are equated, resulting in a systematic calculation that is outlined next.

Order ϵ^{-5}: The leading order problem reads

$$(B^{(0)}\theta_z^{(0)})_z = 0, \quad B^{(0)} = (\theta_z^{(0)})^2, \quad M^{(1)} = -\theta_{zz}^{(0)} \tag{22}$$

whose solution is given by integration and use of the matching condition $\theta^{(0)}(z)_z \sim 0$, $z \to \pm\infty$. We obtain

$$\theta^{(0)} = \Phi(s, t), \quad B^{(0)} = 0, \quad M^{(1)} = 0, \tag{23}$$

where $\Phi(s, t)$ is (by matching) the limiting value of the outer solution Θ as $r \to 0$. Since Θ solves (5), it follows that $\Phi_s^2 + \Theta_r^2 = 1$ on the boundary, and in particular

$$0 \le |\Phi_s| \le 1. \tag{24}$$

Φ_s corresponds to the strength of the grain boundary energy. When $\Phi_s \approx 0$, the jump in $\nabla\Theta$ across the boundary is large, corresponding to a sharp angle between contours of Θ, whereas when $\Phi_s \approx 1$, the jump in $\nabla\Theta$ is nearly zero. Order ϵ^{-4} is omitted because it yields nothing.

Order ϵ^{-3}: The only informative relation at this level is

$$B^{(1)} = 2\theta_z^{(0)}\theta_z^{(1)} = 0. \tag{25}$$

Order ϵ^{-2}: At this level, the structure of the grain boundary is found by solving

$$0 = M_{zz}^{(1)} + (B^{(2)}\theta_z^{(1)})_z, \quad B^{(2)} = (\theta_z^{(1)})^2 + \Phi_s^2 - 1, \quad M^{(1)} = -\theta_{zz}^{(1)} \tag{26}$$

which leads to the single equation

$$-\theta_{zzzz}^{(1)} + ([(\theta_z^{(1)})^2 + \Phi_s^2 - 1]\theta_z^{(1)})_z = 0. \tag{27}$$

Using the matching condition $\theta^{(1)}(z)_{zz} \sim 0, z \to \pm\infty$ (see Eq. (42)), we can integrate this equation directly and obtain the exact self-dual"knee" solutions [7,20] that describe the structure of the grain boundary:

$$\theta^{(1)} = \sigma\sqrt{2}\ln\cosh\left(\sqrt{\frac{1-\Phi_s^2}{2}}z\right) + C(s,t) \equiv \sigma\,\Psi_{\pm}(z;\,\Phi) + C. \tag{28}$$

The sign σ is negative for grain boundaries that are ridges and positive for those which are valleys. The term C arises as a constant of integration. For reference we also have

$$-\sqrt{2}\,\Psi_{zz} = B^{(2)} = (\Phi_s^2 - 1)\mathrm{sech}^2\left(\sqrt{\frac{1-\Phi_s^2}{2}}z\right). \tag{29}$$

Order ϵ^{-1}: At this order we obtain a linear problem for $\theta^{(2)}$

$$\mathcal{L}\theta^{(2)} = -\sigma\kappa(-2\,\Psi_{zzz} - 2\,\Phi_s^2(z\,\Psi_z)_z + B^{(2)}\,\Psi_z) + 2\,\Phi_s([\,\Psi + \sigma C]_s\,\Psi_z)_z + (B^{(2)}\,\Phi_s)_s \tag{30}$$

where

$$\mathcal{L} = \frac{\partial^4}{\partial z^4} - \frac{\partial}{\partial z}[3\,\Psi_z^2 + \Phi_s^2 - 1]\frac{\partial}{\partial z}. \tag{31}$$

The nullspace of the self-adjoint operator $\mathcal{L}$ is spanned by the set $\{1,\ \Psi_z\}$. Roughly speaking, these eigenfunctions correspond to the invariance of energy with respect to vertical displacement of Φ and horizontal motion of the grain boundary, respectively. Note that the terms multiplying the curvature in (30) are odd functions of z, and the other terms on the right hand side are even. The former will therefore drop away when performing the inner product with 1, and the latter will vanish when performing an inner product with Ψ_z.

The first solvability condition is obtained by integrating (30) from $-Z$ to Z and computing the asymptotics as $Z \to \infty$. Using the matching condition $\theta^{(2)}(z)_{zzz} \sim 0, z \to \pm\infty$ (see Eq. (42)) and symmetry, integration gives

$$-(3\,\Psi_z^2(Z) + \Phi_s^2 - 1)[\theta_z^{(2)}]_{-Z}^{Z} + o(1) = 2\,\Phi_s[\,\Psi(Z) + \sigma C]_s[\,\Psi_z]_{-Z}^{Z} - \sqrt{2}(\Phi_s[\,\Psi_z]_{-Z}^{Z})_s \tag{32}$$

where we have used $B^{(2)} = -\sqrt{2}\,\Psi_{zz}$. As $Z \to \infty$,

$$\Psi_z\,\Psi_s = -Z\tanh^2\left(\sqrt{\frac{1-\Phi_s^2}{2}}z\right)\Phi_{ss}\,\Phi_s \sim -Z\,\Phi_{ss}\,\Phi_s + o(1) \tag{33}$$

$$\Psi_z^2 \sim 1 - \Phi_s^2, \tag{34}$$

and therefore

$$[\theta_z^{(2)}]_{-Z}^{Z} \sim 2Z\frac{\Phi_{ss}\,\Phi_s^2}{1-\Phi_s^2} + \sqrt{2}\frac{(\Phi_s\sqrt{1-\Phi_s^2})_s}{1-\Phi_s^2} - \frac{2\sigma\,\Phi_s C_s}{\sqrt{1-\Phi_s^2}}. \tag{35}$$

The second solvability condition is obtained by multiplication of (30) by Ψ_z and integrating from $-Z$ to Z. Using symmetry again, the large Z asymptotics are

$$\begin{aligned}-[3\,\Psi_z^2 + \Phi_s^2 - 1]\,\Psi_z(Z)[\theta_z^{(2)}(Z) + \theta_z^{(2)}(-Z)] + o(1) &= -2\sigma\kappa\int_{-Z}^{Z} -\Psi_{zzz}\,\Psi_z - \Phi_s^2(z\,\Psi_z)_z\,\Psi_z - \frac{\sqrt{2}}{2}\,\Psi_{zz}\,\Psi_z^2\mathrm{d}z \\ &\equiv \kappa(I_1 + I_2 + I_3).\end{aligned} \tag{36}$$

The first and third integrals converge for large Z:

$$I_1 \sim \int_{-\infty}^{\infty}\Psi_{zz}^2\mathrm{d}z = \frac{2\sqrt{2}}{3}(1-\Phi_s^2)^{\frac{3}{2}} \tag{37}$$

$$I_3 \sim -\frac{\sqrt{2}}{3}(1-\Phi_s^2)^{\frac{3}{2}}. \tag{38}$$

The second integral can be integrated by parts to give

$$I_2 \sim -2Z\,\Phi_s^2(1-\Phi_s^2) + \Phi_s^2\int_{-\infty}^{\infty} z\,\Psi_z\,\Psi_{zz}\mathrm{d}z + o(1) = -2Z\,\Phi_s^2(1-\Phi_s^2) + \sqrt{2}\,\Phi_s^2\sqrt{1-\Phi_s^2} + o(1). \tag{39}$$

As $Z \to \infty$ in Eq. (36),

$$\theta_z^{(2)}(Z) + \theta_z^{(2)}(-Z) \sim -Z\frac{2\sigma\kappa\,\Phi_s^2}{\sqrt{1-\Phi_s^2}} + \sigma\kappa\left(\frac{\sqrt{2}}{3} + \frac{\sqrt{2}\,\Phi_s^2}{1-\Phi_s^2}\right). \tag{40}$$

Combining the results of (35) and (40) yields the asymptotic behavior

$$\begin{aligned}\theta_z^{(2)}(Z,s,t) \sim\ & Z\left(\frac{\Phi_{ss}\,\Phi_s^2}{1-\Phi_s^2} \mp \frac{\sigma\kappa\,\Phi_s^2}{\sqrt{1-\Phi_s^2}}\right) \pm \frac{\sqrt{2}}{2}\frac{(\Phi_s\sqrt{1-\Phi_s^2})_s}{1-\Phi_s^2} \\ & + \sigma\kappa\left(\frac{\sqrt{2}}{6} + \frac{\sqrt{2}}{2}\frac{\Phi_s^2}{1-\Phi_s^2}\right) \mp \frac{\sigma\,\Phi_s C_s}{\sqrt{1-\Phi_s^2}}, \quad Z \to \pm\infty.\end{aligned} \tag{41}$$

3.3. Matching and grain boundary dynamics

The dynamics of Φ and the motion of the grain boundary are now determined by matching the inner and outer solutions. The relevant matching conditions take the form of large z asymptotics for the inner solution:

$$\theta^{(0)}(z,s,t) \sim \Theta(0,s,t) \tag{42}$$

$$\theta^{(1)}(z,s,t) \sim \Theta_r(0,s,t)z + \Theta^{(1)}(0,s,t) \tag{43}$$

$$\theta^{(2)}(z,s,t) \sim \frac{1}{2}\Theta_{rr}(0,s,t)z^2 + \Theta_r^{(1)}(0,s,t)z + \Theta^{(2)}(0,s,t). \tag{44}$$

The first two imply

$$\Theta(0,s,t) = \Phi(s,t), \quad \Theta^{(1)}(0,s,t) = C(s,t). \tag{45}$$

Differentiating the third matching condition with respect to r and using (41) we obtain

$$\Theta_{rr} = \frac{\Phi_{ss}\,\Phi_s^2}{1-\Phi_s^2} - \frac{\sigma\kappa\,\Phi_s^2}{\sqrt{1-\Phi_s^2}} \tag{46}$$

$$\Theta_r^{(1)} = \frac{\sqrt{2}}{2}\frac{(\Phi_s\sqrt{1-\Phi_s^2})_s}{1-\Phi_s^2} + \sigma\kappa\left(\frac{\sqrt{2}}{6} + \frac{\sqrt{2}}{2}\frac{\Phi_s^2}{1-\Phi_s^2}\right) - \frac{\sigma\,\Phi_s C_s}{\sqrt{1-\Phi_s^2}} \tag{47}$$

valid as $r \to 0^+$. The first expression (46) merely demonstrates consistency with the outer solution. Writing (5) in the (r,s) coordinates gives

$$(\Theta_r)^2 + (1 + 2\kappa r + \mathcal{O}(r^2))(\Theta_s)^2 = 1. \tag{48}$$

Differentiating this and setting $r = 0$ gives

$$\Theta_{rr}\,\Theta_r + \kappa\,\Theta_s^2 + \Theta_{rs}\,\Theta_s = 0, \quad \Theta_{rs}\,\Theta_r + \Theta_{ss}\,\Theta_s = 0. \tag{49}$$

Solving for $\Theta_{rr}(0,s,t)$ gives exactly formula (46).

Combining the second condition (47) with the matching conditions (45), the terms involving C cancel, giving

$$\begin{aligned}\nabla\Theta\cdot\nabla\Theta^{(1)} &= \Theta_r\,\Theta_r^{(1)} + \Theta_s\,\Theta_s^{(1)} \\ &= \sigma\frac{\sqrt{2}}{2}\frac{(\Phi_s\sqrt{1-\Phi_s^2})_s}{\sqrt{1-\Phi_s^2}} + \kappa\left(\frac{\sqrt{2}}{6}\sqrt{1-\Phi_s^2} + \frac{\sqrt{2}}{2}\frac{\Phi_s^2}{\sqrt{1-\Phi_s^2}}\right)\end{aligned} \tag{50}$$

where $\Theta_r = \sigma\sqrt{1-\Phi_s^2}$ was used. Using expression (15), the dynamics on each characteristic $\ell(\gamma)$ are therefore

$$|\ell|\,\Theta_t = -\left(\frac{\sqrt{2}(\Phi_s\sqrt{1-\Phi_s^2})_s}{\sqrt{1-\Phi_s^2}}G^{-1}\right)_{x(\gamma)}^{\tilde{x}(\gamma)} - \left[\kappa\left(\frac{\sqrt{2}}{3}\sqrt{1-\Phi_s^2} + \frac{\sqrt{2}\,\Phi_s^2}{\sqrt{1-\Phi_s^2}}\right)G^{-1}\right]_{x(\gamma)}^{\tilde{x}(\gamma)} \tag{51}$$

where $(\cdot)_a^b$ denotes the sum of quantities evaluated at a and b (because of this notation, σ drops away).

Finally, the evolution of the grain boundary itself can be found. Note that in the moving coordinate system (r,s), the total time derivative of Θ found in Eq. (51) can be written

$$\frac{D\Theta}{Dt} = \frac{\partial\Theta}{\partial t} + \frac{\partial\Theta}{\partial s}\frac{\mathrm{d}s}{\mathrm{d}t} + \frac{\partial\Theta}{\partial r}\frac{\mathrm{d}r}{\mathrm{d}t}. \tag{52}$$

Let $V_{\mathbf{n}}$ be the normal velocity of the grain boundary interface of Ω_n and Ω_m, directed so that $V_{\mathbf{n}} > 0$ if the boundary moves toward Ω_m. It follows that $V_{\mathbf{n}} = r_t$ by the choice of the coordinate r. Using $\Theta_r(0^{\pm}, s, t) = \pm\sigma\sqrt{1-\Phi_s^2}$ and taking the sum and difference of (52) across the boundary, matching implies

$$\left.\frac{\partial\Theta}{\partial t}\right|_r = \frac{\partial\Phi}{\partial t} + \frac{\partial\Phi}{\partial s}\frac{\mathrm{d}s}{\mathrm{d}t} = \frac{1}{2}((\Theta_n)_t + (\Theta_m)_t), \tag{53}$$

$$V_{\mathbf{n}} = \frac{\sigma}{2\sqrt{1-\Phi_s^2}}((\Theta_n)_t - (\Theta_m)_t). \tag{54}$$

Here Θ_n refers to the outer solution on grain Ω_n, whose time derivative is computed using (51).

The following picture has emerged. For any point $x = x_n(s) = x_m(s)$ on a grain boundary between grains Ω_n, Ω_m, there are two characteristic curves $\ell_{n,m} \in \Omega_{n,m}$ so that $x(s)$ is an endpoint of each of them. The other endpoints of $\ell_{n,m}$ are the *conjugate points* $\tilde{x}_n(s)$, $\tilde{x}_m(s)$ that lie on adjacent grain boundaries (see Fig. 5). It follows from (51), (53) and (54) that $\mathrm{d}\Phi/\mathrm{d}t$ and the normal velocity of the boundary depend on data at x, $\tilde{x}_n$ and $\tilde{x}_m$ involving the curvature of the grain boundary and derivatives of Φ.

4. Grain boundary junctions

Because the dynamics along curves are functions of spatial derivatives of dependent quantities (Φ and curve position), a complete description of events requires conditions at end points along the grain boundary curves. This could either be at physical boundaries, at terminal points where the grain boundary simply vanishes into the bulk, or at junctions where several grain boundaries meet. The focus here will be on the latter.

Because of the problem's variational property, it is natural to imagine that conditions at junctions arise from local energy minimization, akin to the Herring conditions [15] in the theory of crystalline grain boundary motion. Our problem is unique in that energy minimization is strongly constrained by the requirement that the hyperbolic eikonal equation must be satisfied on grain interiors. This gives rise to the possibility of conditions which are not necessarily local to each junction, but allow for communication along characteristics.

Numerical observations suggest at least two standard types of junctions: saddle junctions, where exactly four grain boundaries meet, and extrema junctions which correspond to minima and maxima of Θ. The latter type appears (see Figs. 1 and 8) to have no obvious preference for the number of grain boundaries which are joined. A standard expansion is used for saddle junctions which is seen to be invalid for extrema junctions. The breakdown of the expansion requires the introduction of a mesoscale boundary layer and a modified calculation for the appropriate junction conditions.

4.1. Saddle junctions

Suppose that the grain boundary curves meet at dynamic junctions points $\{\mathbf{x}_k(t)\}$, and define $J_k = \{i | \mathbf{x}_k \in \Gamma_i\}$ as the set of indices of grain boundaries that meet at $\mathbf{x}_k$. We seek a solution to (1) in the rescaled moving coordinate $y = (\mathbf{x} - \mathbf{x}_k(t))/\epsilon$. Expanding Θ as the series $\theta^{(0)} + \epsilon\theta^{(1)} + \epsilon^2\theta^{(2)} + \ldots$, we obtain the leading order behavior $|\nabla\theta^{(0)}| = 0$, so $\theta^{(0)} =$ constant. At next order a nonlinear problem emerges for $\theta^{(1)} \equiv \psi$:

$$-\Delta^2\psi + \nabla\cdot([|\nabla\psi|^2 - 1]\nabla\psi) = 0. \tag{55}$$

This expresses the fact that on the $\mathcal{O}(1)$ timescale, junctions represent local equilibria of the energy (2). Eq. (55) only has solutions for certain far-field boundary conditions. This can be cast in terms of "nonlinear" solvability conditions (see e.g. [10,27]) that arise from taking the inner product of (55) with 1 and $\nabla\psi$ that correspond to the gauge and translation symmetries of the energy. The inner product being zero is equivalent to the energy being stationary with respect to these perturbations. This places restrictions on the far-field conditions which are then matched to the grain boundaries. The same philosophy will be employed in Section 4.2.

Let P be a polygon, centered at $y = 0$, with sides S_i normal to the tangential direction of the grain boundaries Γ_i at $\mathbf{x}_k$ (see Fig. 6). We are interested in the limit as the boundary of the polygon is taken to infinity. Corresponding to each side S_i is a local rectilinear coordinate system (z, q) chosen so that the z coordinate coincides with that for the grain boundary Γ_i, and $q = s/\epsilon$ is the rescaled arclength coordinate along the grain boundary. For all junction conditions, we adopt the convention that s is always directed positive in the direction toward the junction. Integrating (55) on P and using the divergence theorem gives an integral along the boundary of P, which can be put in terms of the z coordinates:

$$0 = \sum_{i\in J_k}\int (\Delta\psi)_q + (|\nabla\psi|^2 - 1)\psi_q \,\mathrm{d}z(S_i). \tag{56}$$

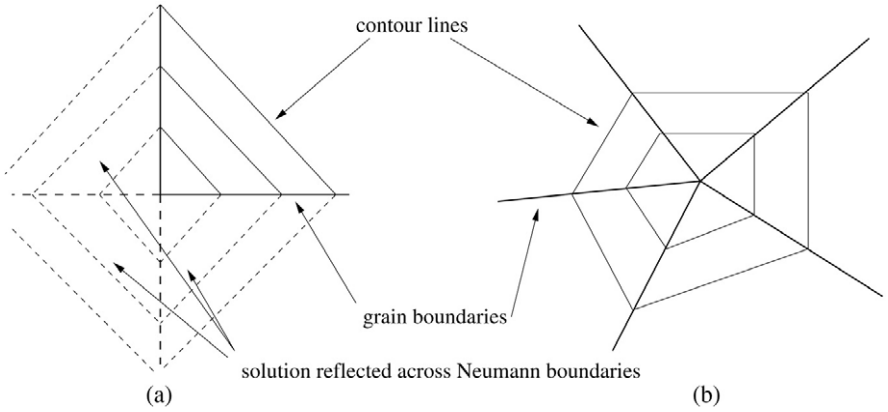

Fig. 8. Extrema junctions. (a) shows the contours for the function $\Theta \sim \sqrt{2}/2(x+y)$ used in the text which yields an extrema junction in a corner of the physical domain by reflection. A more generic example is given in (b). In general there is no preferred angle between adjacent grain boundaries at these junctions.

Taking the boundary of P to infinity is the same as taking the integrals over z in this expression from $-\infty$ to ∞. We can match the junction solution onto each grain boundary solution by use of conditions similar to (42), giving

$$(\Delta\psi)_q \sim 0, \quad \psi_q \sim \Phi_s(s_0,t), \quad \psi_z \sim \Psi_z(z,s_0,t), \quad q \to \infty \tag{57}$$

where $x(s_0) = x_k$. Therefore (56) can be written

$$0 = \sum_{i\in J_k} \int_{-\infty}^{\infty} \Phi_s(\Psi^2 + \Phi_s^2 - 1)\mathrm{d}z(S_i). \tag{58}$$

Using the explicit solution (28), this integrates to the first junction condition

$$\sum_{i\in J_k} (\Phi_i)_s \sqrt{1-(\Phi_i)_s^2} = 0. \tag{J1}$$

Here Φ_i, Ψ_i refers to the limiting value of functions or derivatives along the grain boundary Γ_i as the junction is approached.

In a similar fashion, (55) can be multiplied by $\nabla\psi$ and integrated over the same polygon. Let $\hat{\mathbf{t}}_i$ be the unit tangent vector of Γ_i at $\mathbf{x}_k$, which is also the normal vector to side S_i of P. A boundary integral can again be obtained:

$$\begin{aligned}
0 &= \int_P (-\Delta^2\psi + \nabla\cdot([|\nabla\psi|^2 - 1]\nabla\psi))\nabla\psi \,\mathrm{d}A \\
&= \int_{\partial P} -(\nabla\Delta\psi\cdot\hat{\mathbf{t}})\nabla\psi + (|\nabla\psi|^2-1)(\nabla\psi\cdot\hat{\mathbf{t}})\nabla\psi + (\Delta\psi)\nabla^2\psi\cdot\hat{\mathbf{t}}\,\mathrm{d}s \\
&\quad - \int_P \nabla\left[\frac{1}{2}(\Delta\psi)^2 + \frac{1}{4}(|\nabla\psi|^2-1)^2\right]\mathrm{d}A \\
&= \int_{\partial P} -(\nabla\Delta\psi\cdot\hat{\mathbf{t}})\nabla\psi + (|\nabla\psi|^2-1)(\nabla\psi\cdot\hat{\mathbf{t}})\nabla\psi + (\Delta\psi)\nabla^2\psi\cdot\hat{\mathbf{t}} \\
&\quad - \left[\frac{1}{2}(\Delta\psi)^2 - \frac{1}{4}(|\nabla\psi|^2-1)^2\right]\hat{\mathbf{t}}\,\mathrm{d}s.
\end{aligned} \tag{59}$$

In the last step, the integrands of the form ∇f were written as a divergence of the tensor $f\mathrm{I}$. The required matching conditions are (57) and

$$(\nabla\psi\cdot\hat{\mathbf{t}})\nabla\psi \sim \Phi_s^2\hat{\mathbf{t}} + \Phi_s\Psi_z\hat{\mathbf{t}}_\perp, \quad \Delta\psi \sim \Psi_{zz}, \quad (\nabla^2\psi)\cdot\hat{\mathbf{t}} \sim 0, \quad q\to\infty \tag{60}$$

where $\hat{\mathbf{t}}_\perp$ is normal to $\hat{\mathbf{t}}$. The computation (59) implies that as the boundary of the polygon goes to infinity,

$$\sum_{i\in J_k} \int_{-\infty}^{\infty} \Phi_s(\Phi_s\hat{\mathbf{t}} + \Psi_z\hat{\mathbf{t}}_\perp)[\Psi_z^2 + \Phi_s^2 - 1] - \left(\frac{1}{2}\Psi_{zz}^2 + \frac{1}{4}[\Psi_z^2 + \Phi_s^2 - 1]^2\right)\hat{\mathbf{t}}\,\mathrm{d}z(S_i) = 0. \tag{61}$$

Inserting the explicit solution (28), the second junction condition is obtained:

$$\sum_{i\in J_k} \left((\Phi_i)_s^2\sqrt{1-(\Phi_i)_s^2} + \frac{1}{3}(1-(\Phi_i)_s^2)^{3/2}\right)\hat{\mathbf{t}}_i = 0. \tag{J2}$$

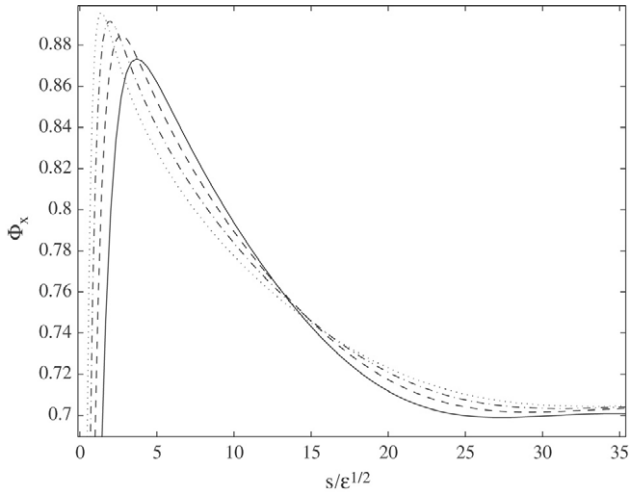

Fig. 9. Plot of Φ_s along the lower boundary of $\Theta \sim \sqrt{2}/2(x+y)$ for $\epsilon = 0.4, 0.2, 0.1, 0.05$ (solid, dash, dash–dot, dotted), showing the presence of a mesoscale boundary layer of size $\sim\epsilon^{1/2}$.

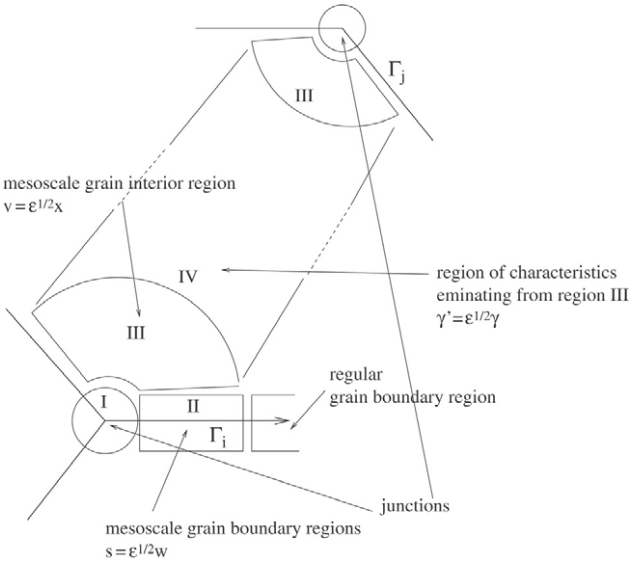

Fig. 10. Diagram of all matched asymptotic regions and their scalings. Two mesoscopic regions are used near each junction corresponding to grain boundaries and grain interiors. Characteristics that emanate from the mesoscale region form a band (region IV) which must connect two junctions.

It is observed in simulations that saddle junctions always meet in a perpendicular fashion with contours of Θ intersecting at an angle of $\pi/2$ (see Fig. 7), so that $\Phi_s = \pm\sqrt{2}/2$. It is easy to see that (J1) and (J2) hold in this case because of the symmetry. More is said about the variational meaning of these conditions in the next section.

4.2. Extrema junctions and the mesoscale expansion

Notice that (J1) is impossible at extrema junctions because Φ_s is always of one sign there. This evidently signifies a breakdown in the asymptotic expansion which leads to this condition. To illustrate this, consider the simple scenario (which turns out to be a global equilibrium) where $\Theta \sim \sqrt{2}/2(x+y)$ on a square domain with reflective boundary conditions. (This was obtained by using $\sqrt{2}/2(x+y)$ as an initial condition and allowing diffuse grain boundaries to form by computing to a steady state.) Grain boundaries form along the edges of the square domain which connect extrema junctions in the southwest and northeast corners to saddle junctions at the other two. Because of the enforced symmetry, the extrema junctions are formed by four grain boundaries meeting at right angles, but this is not generically the case (see Fig. 8). A direct measurement of $\Phi_s = \Theta_x(s,0)$ from a simulation of (1) shows the presence of a boundary layer near the extrema junctions. Scaling lengths by $\epsilon^{1/2}$ shows a collapse of Φ_s onto a single curve near the junction (see Fig. 9), suggesting that an intermediate region is needed in our asymptotic expansion.

The following matched expansion picture is proposed (see Fig. 10). Very close to the junction point (region I), the coordinate $y = (\mathbf{x} - \mathbf{x}_k(t))/\epsilon$ is used as before. Along each phase grain boundary and near each junction (region II), the coordinates

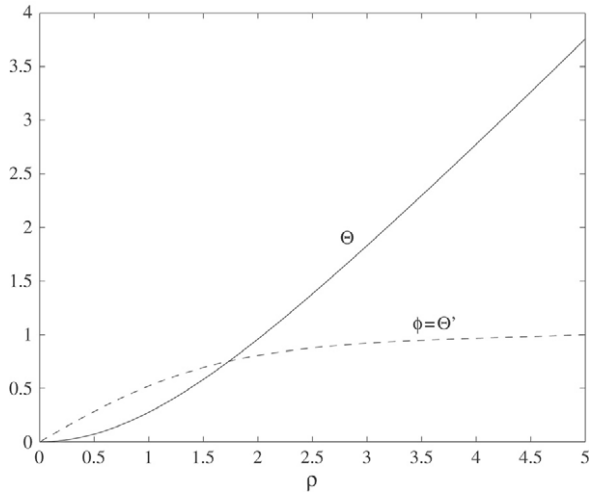

Fig. 11. Numerical computation of radially symmetric solution on asymptotic region I.

(z, w), $w = \epsilon^{-1/2}s$ are used. Away from the phase grain boundaries but within an $\mathcal{O}(\epsilon^{1/2})$-size region near the junctions (region III), the coordinate $\mathbf{v} = (\mathbf{x} - \mathbf{x}_k(t))/\epsilon^{1/2}$ is used. At extrema junctions, eikonal characteristics parallel to $\nabla\Theta$ emanate from this mesoscale region along a band (region IV) in the grain bulk. Proper matching requires a modification of the outer expansion along this band, and moreover it is argued below that the other end of this band must also connect to an extrema junction.

In region I, the leading order solution satisfies (55) as before. The difference is in the far field behavior. Repeating the argument of integrating over a polygonal region, we find that in the direction of phase grain boundaries, $|\nabla\Theta|$ must tend toward one in the far field to admit an extrema type solution. In fact, this must be true in every direction, because (as shown below) the solution needs to match an eikonal solution in region III. This suggests that the solution in this region has radial symmetry, which appears to coincide with numerical observation. Radial solutions $\Theta = \Theta(\rho)$, $\rho = |y|$ satisfy

$$\left(-\rho\left[\frac{1}{\rho}(\rho\Theta')'\right]' + \rho[(\Theta')^2 - 1]\Theta'\right)' = 0. \tag{62}$$

Matching requires $\nabla\Delta\Theta$, $|\nabla\Theta|^2 - 1 \to 0$ for large ρ, so that by integrating a boundary value problem for $\phi = \Theta'$ is obtained:

$$\phi'' + \left(\frac{\phi}{\rho}\right)' - (\phi^2 - 1)\phi = 0, \quad \phi(0) = 0, \quad \phi(\infty) = 1. \tag{63}$$

Fig. 11 shows a numerical solution of this problem using an elementary shooting method.

In region II, the coordinate s is rescaled to $w = \epsilon^{-1/2}s$ to reflect the observed boundary layer in Φ_s. The mesoscale grain boundary expansion (denoted by subscript m) will have the form

$$\theta = \epsilon^{1/2}\theta_m^{(1/2)}(z, w, t) + \epsilon\theta_m^{(1)}(z, w, t) + \epsilon^{3/2}\theta_m^{(3/2)}(z, w, t)\ldots. \tag{64}$$

The calculation is almost the same as that of Section 3.2, so it will not be repeated in detail. The primary difference is that the curvature terms do not appear in the leading order solvability condition, since we still assume that κ is $\mathcal{O}(1)$. We are led to the analog of the asymptotic behavior (41) which reads

$$\theta_m^{(3/2)}(Z, w, t) \sim Z\left(\frac{\Phi_{ww}\Phi_w^2}{1 - \Phi_w^2}\right) \pm \frac{\sqrt{2}}{2}\frac{(\Phi_w\sqrt{1 - \Phi_w^2})_w}{1 - \Phi_w^2} \mp \frac{\sigma\Phi_w C_w}{\sqrt{1 - \Phi_w^2}}, \quad Z \to \pm\infty \tag{65}$$

where $\Phi(w, t) = \theta^{(1/2)}$ is the leading order behavior.

In region III, the rescaling $\mathbf{v} = (\mathbf{x} - \mathbf{x}_k(t))/\epsilon^{1/2}$ is employed, together with the expansion

$$\Theta = \epsilon^{1/2}\Theta_m^{(1/2)}(\mathbf{v}, t) + \epsilon\Theta_m^{(1)}(\mathbf{v}, t) + \cdots. \tag{66}$$

Again the details are similar to the earlier calculation of Section 3.1. The leading order solutions solve $|\nabla\Theta_m^{(1/2)}|^2 = 1$, but some caution is necessary here. To match onto the region I solution, $\Phi_v \to 1$ as the junction is approached. This means that in region III, as the junction is approached, eikonal characteristics that terminate on the grain boundary must become parallel to the grain boundary itself (Fig. 12). Within each grain, therefore, there is a "connection" region where all characteristics terminate at the

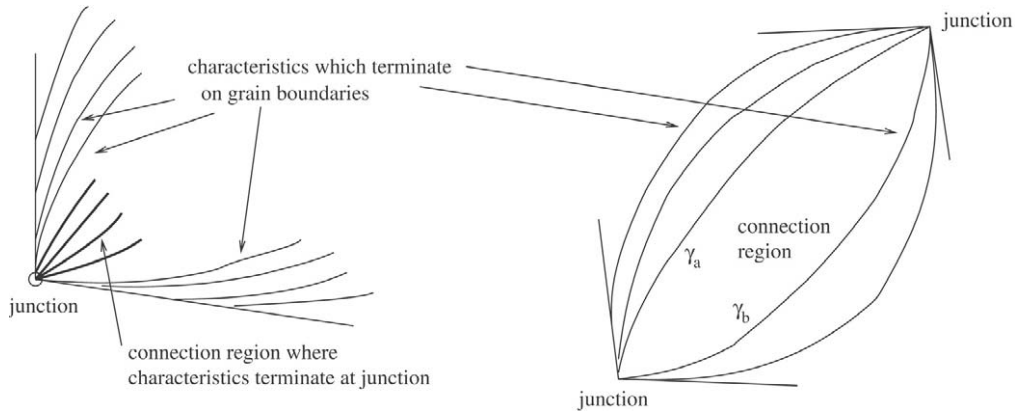

Fig. 12. Left: In region III, characteristics necessarily become parallel to the grain boundary as the junction is approached. The connection region is formed where all characteristics intersect the junction. Right: connection region characteristics must terminate at two adjacent extrema junctions.

junction point itself. The correction in the expansion satisfies the steady version of Eq. (8) which reads

$$\nabla \cdot ([\nabla \Theta_m^{(1/2)} \cdot \nabla \Theta_m^{(1)}] \nabla \Theta_m^{(1/2)}) = 0. \tag{67}$$

It is useful to use a rescaled version of the characteristic coordinate system $(\chi_m, \gamma_m) = \epsilon^{1/2}(\chi, \gamma)$ to emphasize the fact that these coordinates range over all values in the context of the expansion. The solvability argument leads to the expression

$$\lim_{|\chi_m| \to \infty} \nabla \Theta_m^{(1/2)} \cdot \nabla \Theta_m^{(1)} G^{-1} = \nabla \Theta_m^{(1/2)} \cdot \nabla \Theta_m^{(1)} G^{-1}|_{x(\gamma)}. \tag{68}$$

Here $x(\gamma)$ is the endpoint of a characteristic curve at a point on a phase grain boundary and $|\chi_m| \to \infty$ refers to the limit as region IV is approached. To avoid confusion, the metric G is defined using the original scaling.

In region IV, the expansion must be $\Theta = \Theta^{(0)} + \epsilon^{(1/2)} \Theta^{(1/2)} + \cdots$ to properly match to region III. Furthermore, the thickness of this region scales like $\mathcal{O}(\epsilon^{1/2})$, so the rescaled characteristic coordinate γ_m is used. The outcome is like that of region III: the leading order solution is the eikonal equation, and the correction term satisfies a steady equation like (67). The solvability argument gives an equilibrium condition

$$[\nabla \Theta^{(0)} \cdot \nabla \Theta^{(1/2)} G^{-1}]_{x(\gamma_m)}^{\tilde{x}(\gamma_m)} = 0 \tag{69}$$

rather than a dynamic one. The points $x(\gamma_m)$, $\tilde{x}(\gamma_m)$ are, as before, the limiting endpoints of the characteristics. Because of the $\epsilon^{1/2}$ scaling of the correction term, it is not possible to match region IV onto a phase grain boundary directly. A nontrivial requirement emerges: *characteristics which emanate from a mesoscale junction region must terminate in another mesoscale junction region.* In other words, in the limit of small ϵ, adjacent maximum and minimum junctions are connected by characteristics. This requirement is consistent with numerical observations (see Fig. 2).

Matching regions III and IV uses the conditions

$$\nabla_v \Theta_m^{(1/2)} \sim \nabla \Theta^{(0)}, \quad \nabla_v \Theta_m^{(1)} \sim \nabla^2 \Theta^{(0)} \cdot \mathbf{v} + \nabla \Theta^{(1/2)}, \quad \mathbf{v} \to \infty. \tag{70}$$

If $\mathbf{v}$ is taken to infinity in the direction of a characteristic curve, then

$$\nabla^2 \Theta^{(0)} \cdot \mathbf{v} \sim \nabla^2 \Theta^{(0)} \cdot \nabla \Theta^{(0)} = 0 \tag{71}$$

because $\Theta^{(0)}$ solves the eikonal equation. Therefore combining (68) and (69) gives

$$[\nabla \Theta_m^{(1/2)} \cdot \nabla \Theta_m^{(1)} G^{-1}]_{x(\gamma_m)}^{\tilde{x}(\gamma_m)} = 0. \tag{72}$$

If γ_m corresponds to a characteristic in the connection region, then $x(\gamma_m)$ is a junction point rather than a point on the grain boundary. Note that the metric G^{-1} necessarily goes to zero at this point, so (72) implies that $\nabla \Theta_m^{(1/2)} \cdot \nabla \Theta_m^{(1)} G^{-1}$ is zero at the other endpoint $\tilde{x}(\gamma_m)$. If $\tilde{x}(\gamma_m)$ is on a grain boundary, then we observe below that $\nabla \Theta_m^{(1/2)} \cdot \nabla \Theta_m^{(1)} \neq 0$, so it must be that G^{-1} is zero at $\tilde{x}(\gamma_m)$. This means that characteristics emanating (in region III) from a junction must also terminate in a junction. The connection region is described by the interval $C = (\gamma_a, \gamma_b)$ so that if $\gamma_m \notin C$, $x(\gamma_m)$, $\tilde{x}(\gamma_m)$ are on grain boundaries (see Fig. 12).

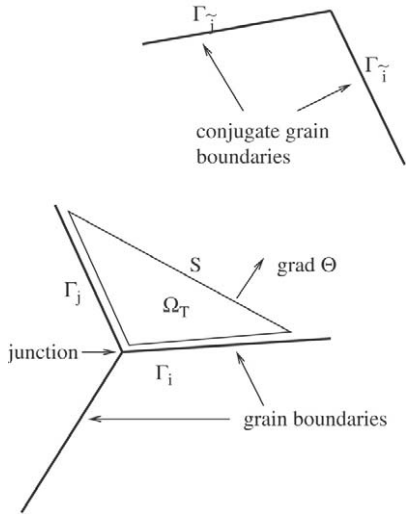

Fig. 13. Triangular region of integration. The integral along S can be written as one along conjugate boundaries.

For these points, matching to region II using (65) produces the analog of (51),

$$\left(\frac{(\Phi_w\sqrt{1-\Phi_w^2})_w}{\sqrt{1-\Phi_w^2}}G^{-1}\right)_{x(\gamma_m)}^{\tilde{x}(\gamma_m)} = 0. \tag{73}$$

Along the boundary, using the metric (6) and the fact $\Theta = \Phi = \chi$ yields $\mathrm{d}s^2 = \Phi_s^2\mathrm{d}s^2 + G^{-2}\mathrm{d}\gamma^2$ and therefore

$$\mathrm{d}s = (1-\Phi_s^2)^{-1/2}G^{-1}\mathrm{d}\gamma. \tag{74}$$

It follows that (73) can be rewritten as

$$\frac{\mathrm{d}}{\mathrm{d}\gamma_m}\left(\Phi_w\sqrt{1-\Phi_w^2}\right)_{x(\gamma_m)}^{\tilde{x}(\gamma_m)} = 0. \tag{75}$$

Integrating this from γ_b to ∞ (or from $-\infty$ to γ_a) and matching to region I and the regular grain boundary gives the nonlocal junction condition

$$(\Phi_i)_s\sqrt{1-(\Phi_i)_s^2} = -(\Phi_{\tilde{i}})_s\sqrt{1-(\Phi_{\tilde{i}})_s^2} \tag{J1′}$$

where Γ_i and $\Gamma_{\tilde{i}}$ are grain boundaries that contain conjugate points (as before s is oriented to be increasing as the junction is approached). Junction condition (J1′) will form one of two replacements for the conditions derived in Section 4.1.

It is now instructive to repeat the argument in Section 4.1 of taking inner products with the functions 1 and $\nabla\Theta$. In the context of the mesoscale expansion, this means taking inner products with the region III correction equation (67), matching and adding the results at each junction to give the "total" inner product at a junction. We do this by integrating on a triangular subregion Ω_T in region III whose sides are formed by the two grain boundaries (which are straight lines in the mesoscale coordinates) and a third side S which is normal to $\mathbf{g} = \nabla\Theta$, evaluated as the junction is approached (see Fig. 13). The side S will be taken to infinity and the solution matched to the outer solution.

The inner product of (67) with 1 yields a boundary integral over the two grain boundaries Γ_i and Γ_j and the side S. As the triangle expands to infinity, this gives by matching to regions II and IV:

$$\begin{aligned}
0 &= \int_{\Gamma_i+\Gamma_j+S}[\nabla\Theta_m^{(1/2)}\cdot\nabla\Theta_m^{(1)}]\nabla\Theta_m^{(1/2)}\cdot\hat{\mathbf{n}}(\partial\Omega_T)\,\mathrm{d}s \\
&= \int_0^\infty \frac{\sqrt{2}}{2}\left((\Phi_i)_w\sqrt{1-(\Phi_i)_w^2}\right)_w \mathrm{d}w + \int_0^\infty \frac{\sqrt{2}}{2}\left((\Phi_j)_w\sqrt{1-(\Phi_j)_w^2}\right)_w \mathrm{d}w \\
&\quad + \int_{-\infty}^\infty \nabla\Theta^{(1/2)}\cdot\nabla\Theta^{(1)}G^{-1}\,\mathrm{d}\gamma_m \equiv I_1 + I_2 + I_3.
\end{aligned} \tag{76}$$

The first two integrals immediately give (by matching to region I and the regular grain boundary)

$$I_1 + I_2 = \frac{\sqrt{2}}{2}\left((\Phi_i)_s\sqrt{1-(\Phi_i)_s^2} + (\Phi_j)_s\sqrt{1-(\Phi_j)_s^2}\right). \tag{77}$$

The third integral can be matched to region IV which connects to a region near the conjugate junction (see Fig. 13). Suppose that the conjugate grain boundaries are $\Gamma_{\tilde{i}}$, $\Gamma_{\tilde{j}}$, so using (72), integrals like I_1 and I_2 are obtained:

$$I_3 = \frac{\sqrt{2}}{2}\left((\Phi_{\tilde{i}})_s\sqrt{1-(\Phi_{\tilde{i}})_w^2} + (\Phi_{\tilde{j}})_s\sqrt{1-(\Phi_{\tilde{j}})_w^2}\right). \tag{78}$$

Using the condition (J1′), it follows that $I_3 = -I_1 - I_2$ which merely verifies that the integral in (76) really is zero.

Taking the inner product of (67) with $\nabla\Theta_m^{(1/2)}$, a boundary integral can also be obtained. Matching as before and using $\nabla\Theta_m^{(1/2)} = \Phi_w\hat{\mathbf{t}} - \sigma\sqrt{1-\Phi_w^2}\hat{\mathbf{n}}$ on the grain boundary, we have

$$\begin{aligned}
0 &= \int_{\Gamma_i+\Gamma_j+S}[\nabla\Theta_m^{(1/2)}\cdot\nabla\Theta_m^{(1)}][\nabla\Theta_m^{(1/2)}\cdot\hat{\mathbf{n}}(\partial\Omega_T)]\nabla\Theta_m^{(1/2)}\,\mathrm{d}s\\
&= \int_0^\infty \frac{\sqrt{2}}{2}\left((\Phi_i)_w\mathbf{t} - \sigma\sqrt{1-(\Phi_i)_w^2}\hat{\mathbf{n}}\right)\left[(\Phi_i)_w\sqrt{1-(\Phi_i)_w^2}\right]_w \mathrm{d}w\\
&\quad + \int_0^\infty \frac{\sqrt{2}}{2}\left((\Phi_j)_w\mathbf{t} - \sigma\sqrt{1-(\Phi_j)_w^2}\hat{\mathbf{n}}\right)\left[(\Phi_j)_w\sqrt{1-(\Phi_j)_w^2}\right]_w \mathrm{d}w\\
&\quad + \mathbf{g}\int\nabla\Theta^{(1/2)}\cdot\nabla\Theta^{(1)}G^{-1}\mathrm{d}\gamma_m = I_4 + I_5 + I_6.
\end{aligned} \tag{79}$$

Integrating the first two and matching gives

$$\begin{aligned}
I_4 + I_5 &= 2\sqrt{2}\left((\Phi_i)_s^2\sqrt{1-(\Phi_i)_s^2} + \frac{1}{3}(1-(\Phi_i)_s^2)^{3/2}\right)\hat{\mathbf{t}}_i\\
&\quad + 2\sqrt{2}\left((\Phi_j)_s^2\sqrt{1-(\Phi_j)_s^2} + \frac{1}{3}(1-(\Phi_j)_s^2)^{3/2}\right)\hat{\mathbf{t}}_j + \text{normal components}.
\end{aligned} \tag{80}$$

The normal components are intentionally suppressed because they cancel when integrals over all mesoscale regions are summed. The third integral in (79) uses (78) and (J1′) to give

$$I_6 = -\mathbf{g}\frac{\sqrt{2}}{2}\left((\Phi_i)_s\sqrt{1-(\Phi_i)_w^2} + (\Phi_j)_s\sqrt{1-(\Phi_j)_w^2}\right). \tag{81}$$

The vector $\mathbf{g}$ can be written as

$$\mathbf{g} = \frac{1}{2}\left((\Phi_i)_w\hat{\mathbf{t}}_i - \sigma\sqrt{1-(\Phi_i)_w^2}\hat{\mathbf{n}}_i\right) + \frac{1}{2}\left((\Phi_j)_w\hat{\mathbf{t}}_j - \sigma\sqrt{1-(\Phi_j)_w^2}\hat{\mathbf{n}}_j\right). \tag{82}$$

The integrals (79) for each mesoscale region surrounding a junction point can now be summed using (80)–(82). Note that normal vectors to a particular grain boundary are defined relative the grain, and therefore the two normal contributions for each grain boundary cancel. The result is the sum

$$\sum_{i\in J_k}(1-(\Phi_i)_s^2)^{3/2}\hat{\mathbf{t}}_i = 0 \tag{J2′}$$

which is a second extrema junction condition.

5. Variational and mechanical interpretation

It should not be surprising that the grain boundary network dynamics inherit a variational structure like that of the original equation (1). This section demonstrates this, lending plausibility to the calculation of the previous section.

For the purposes of this section, we choose periodic boundary conditions for definiteness. This avoids consideration of the interaction of physical and grain boundaries. Reflective boundary conditions are also covered because four-fold reflection of the solution satisfies periodic boundary conditions.

We can associate a line energy to a grain boundary by using the knee-type solution (28). The energy per unit length (2) of this solution is

$$e = \int_{-\infty}^{\infty} \frac{1}{2}(\theta_{zz}^{(1)})^2 + \frac{1}{4}(\Psi_z^2 + \Phi_s^2 - 1)^2 \, \mathrm{d}z = \frac{2\sqrt{2}}{3}(1 - \Phi_s^2)^{3/2}. \tag{83}$$

Consider a network of grain boundaries $\{\Gamma_i\}$, $i = 1, \ldots, n$, each parameterized (not necessarily with respect to arclength) by curves $\mathbf{x} = \mathbf{x}(\xi)$. In terms of the tangent vector $\mathbf{t}_i = \mathrm{d}\mathbf{x}/\mathrm{d}\xi$,

$$\mathrm{d}s = |\mathbf{t}|\mathrm{d}\xi \qquad \Phi_s = |\mathbf{t}|^{-1}\Phi_\xi. \tag{84}$$

The total grain boundary energy can be defined as the integral of (2) along every boundary

$$E = \frac{2\sqrt{2}}{3}\sum_i \int_{\Gamma_i} (1 - \Phi_s^2)^{3/2} \, \mathrm{d}s = \frac{2\sqrt{2}}{3}\sum_i \int_{\Gamma_i} (1 - |\mathbf{t}|^{-2}\Phi_\xi^2)^{3/2}|\mathbf{t}|\mathrm{d}\xi. \tag{85}$$

This energy (85) is conjectured [2] to be the Γ-limit of the original functional (2) in two dimensions.

5.1. Geometry of the attracting manifold

The fact that the eikonal equation is satisfied within each grain places strong constraints on the allowable values of Φ and locations of the grain boundaries. The set of allowable configurations can be thought of as a manifold $\mathcal{M}$ whose elements $\eta = \{\Phi(\xi), \mathbf{x}(\xi)\}$ are defined implicitly by

$$\Phi(\xi) = \Theta(\mathbf{x}(\xi)) \quad \text{for some } \Theta \text{ satisfying } |\nabla\Theta(\mathbf{x})|^2 = 1, \mathbf{x} \neq \mathbf{x}(\xi). \tag{86}$$

Note that this implies Θ is continuous across grain boundaries.

The tangent space of this manifold can be identified with the set of infinitesimal perturbations $\eta' = \{\Phi'(\xi), \mathbf{x}'(\xi)\}$ chosen so that property (86) is retained. If Θ' is the corresponding perturbation in Θ, then

$$\nabla\Theta \cdot \nabla\Theta' = 0, \quad \mathbf{x} \neq \mathbf{x}(\xi). \tag{87}$$

In terms of the natural characteristic coordinate system (γ, χ) induced by Θ, this means that $\Theta' = \Theta'(\gamma)$ is constant valued along characteristics $\ell(\gamma)$ (it needn't be continuous across grain boundaries, however). Supposing that $x(\gamma), \tilde{x}(\gamma)$ are endpoints of the characteristic $\ell(\gamma)$, the perturbation of (86) reads

$$\begin{aligned}\Phi' &= \Theta'(\mathbf{x}(\xi)) + \nabla\Theta(\mathbf{x}(\xi)) \cdot \mathbf{x}'(\xi) \\ &= \Theta'(\mathbf{x}(\xi)) - \sigma\sqrt{1 - \Phi_s^2}(\mathbf{x}'(\xi) \cdot \hat{\mathbf{n}}) + \Phi_s(\mathbf{x}'(\xi) \cdot \mathbf{t}), \quad \mathbf{x} = x(\gamma), \tilde{x}(\gamma)\end{aligned} \tag{88}$$

where Θ', $\nabla\Theta(\mathbf{x})$ are the limiting values along ℓ at the endpoints. Since Θ' is constant along ℓ, it follows that

$$\Phi' - \sigma\sqrt{1 - \Phi_s^2}(\mathbf{x}' \cdot \hat{\mathbf{n}}) + \Phi_s(\mathbf{x}'(\xi) \cdot \mathbf{t})|_{x(\gamma)} = \Phi' - \sigma\sqrt{1 - \Phi_s^2}(\mathbf{x}' \cdot \hat{\mathbf{n}}) + \Phi_s(\mathbf{x}'(\xi) \cdot \mathbf{t})|_{\tilde{x}(\gamma)}. \tag{89}$$

This defines a linear subspace T_η of all possible values of $\eta' = \{\Phi'(\xi), \mathbf{x}'(\xi)\}$.

The tangent space can be endowed with a metric which it inherits from the native L^2 gradient flow of (1). Given $\eta' \in T_\eta$, one can unambiguously find the perturbation of Θ on each grain Ω_n along a characteristic curve $\ell(\gamma)$ as

$$\Theta_n'(\gamma) = \Phi' - \sigma\sqrt{1 - \Phi_s^2}(\mathbf{x}' \cdot \hat{\mathbf{n}}) + \Phi_s(\mathbf{x}' \cdot \mathbf{t}), \quad \mathbf{x} = x(\gamma) \text{ or } \tilde{x}(\gamma). \tag{90}$$

The metric on T_η arises simply by restriction of L^2 to the manifold $\mathcal{M}$. It is the quadratic form

$$(\eta', \eta')_{g(\eta)} = \sum_n \int_{\Omega_n} (\Theta_n')^2 \mathrm{d}x. \tag{91}$$

The subscript $g(\eta)$ simply denotes the fact that the metric varies at each point η along the manifold.

5.2. Variation of the grain boundary energy

Consider a perturbation satisfying (89) of the form $\mathbf{x}_\varepsilon = \mathbf{x}(\xi) + \varepsilon\mathbf{x}'(\xi)$, $\Phi_\varepsilon = \Phi + \varepsilon\Phi'$, with $\mathbf{t}_\varepsilon = \mathbf{t} + \varepsilon\mathrm{d}\mathbf{x}'/\mathrm{d}\xi$. Inserting these into the energy (85) and computing the derivative with respect to ε gives the variation of E. Setting ξ equal to arclength reduces the

expression to

$$\langle \delta E, \eta' \rangle = \frac{\mathrm{d}E}{\mathrm{d}\varepsilon}(0) = \sum_i \int_{\Gamma_i} R\,\Phi_s' + \mathbf{T}\cdot\mathbf{x}_s'\,\mathrm{d}s \tag{92}$$

where

$$R = -2\sqrt{2}\,\Phi_s\sqrt{1-\Phi_s^2}, \tag{93}$$

$$\mathbf{T} = \left(2\sqrt{2}\,\Phi_s^2\sqrt{1-\Phi_s^2} + \frac{2\sqrt{2}}{3}(1-\Phi_s^2)^{3/2}\right)\hat{\mathbf{t}}, \tag{94}$$

and $\hat{\mathbf{t}} = \mathrm{d}\mathbf{x}/\mathrm{d}s$ is the unit tangent vector. The quantity $\mathbf{T}$ has the mechanical analogy of a line tension because it multiplies the curve strain vector $\mathbf{x}_s'$. The quantity R can be thought of similarly as the "bending" tension because Φ_s determines the amount which contours of Θ bend at the grain boundary.

Integration by parts in (92) gives the variation as a sum over both boundaries and junction points as

$$\langle \delta E, \eta' \rangle = -\sum_i \int_{\Gamma_i} R_s\,\Phi' + \mathbf{T}_s\cdot\mathbf{x}'\,\mathrm{d}s + \sum_k \sum_{i\in J_k} R_i\,\Phi_i' + \mathbf{T}_i\cdot\mathbf{x}_i'. \tag{95}$$

Here $R_i, \mathbf{T}_i, \Phi_i', \mathbf{x}_i'$ are the limits of the respective quantities on the grain boundary Γ_i as the junction point is approached. As before, R_i is computed with s increasing toward the junction point. It is supposed that the junction persists under any perturbation (i.e. we are assuming only stable junctions) and therefore $\Phi_i', \mathbf{x}_i'$ must be the same for all $i \in J_k$. By invoking the junction conditions, we can show that the sum over junction points in (95) is zero. For saddle junctions, (J1) and (J2) are the same as the "force balance"

$$\sum_{i\in J_k} R_i = 0, \quad \sum_{i\in J_k} \mathbf{T}_i = 0 \tag{96}$$

which leads to zero contributions in (95) at these junctions.

The argument for extrema junctions $k \in J_{\mathrm{ex}}$ is more involved. Denote by $P = \{(i,j)\}$ the set of all ordered grain boundary pairs where Γ_i, Γ_j which are conjugate, i.e. have characteristic endpoints in common. Condition (J1′) and constraint (89) can be invoked to rewrite the sum as one over these pairs

$$\begin{aligned}\sum_{k\in J_{ex}} \sum_{i\in J_k} R_i\,\Phi_i' &= \frac{1}{2}\sum_{(i,j)\in P} R_i(\Phi_i' - \Phi_j') \\ &= \frac{1}{2}\sum_{(i,j)\in P} R_i\sigma_i\left(\sqrt{1-(\Phi_i)_s^2}(\mathbf{x}_i'\cdot\hat{\mathbf{n}}_{ij}) + \sqrt{1-(\Phi_j)_s^2}(\mathbf{x}_j'\cdot\hat{\mathbf{n}}_{ij})\right) - R_i(\Phi_i)_s(\mathbf{x}_i'\cdot\mathbf{t}_i) + R_j(\Phi_j)_s(\mathbf{x}_j'\cdot\mathbf{t}_j).\end{aligned} \tag{97}$$

The normal $\hat{\mathbf{n}}_{ij}$ is outward with respect to the grain common to Γ_i and Γ_j. Since (i,j) are ordered pairs, (j,i) is also in P. As a consequence, the sum over normal components in (97) is zero, because $R_i\sigma_i\mathbf{x}_i'\cdot\hat{\mathbf{n}}_{ij} = -R_j\sigma_j\mathbf{x}_i'\cdot\hat{\mathbf{n}}_{ji}$, implying pairwise cancellation of terms. The sum can now revert to one over junctions instead of grain boundary pairs, giving

$$\sum_k \sum_{i\in J_k} R_i\,\Phi_i' + \mathbf{T}_i\cdot\mathbf{x}_i' = \frac{2\sqrt{2}}{3}\sum_k\sum_{i\in J_k}(1-(\Phi_i)_s^2)^{3/2}(\mathbf{x}_i'\cdot\mathbf{t}_i) \tag{98}$$

which is zero because of junction condition (J2′).

5.3. Variational characterization of the limiting dynamics

Finally, we can observe that the gradient flow structure is preserved in the singular limit. A gradient flow on a manifold satisfies the weak equation [12,23]

$$(\eta', \eta_t)_{g(\eta)} = -\langle \delta E, \eta' \rangle \quad \text{for all } \eta' \in T_\eta. \tag{99}$$

Using (91), the definition of $|\ell|$ and the fact that Θ_t, Θ' are constant along each curve ℓ gives

$$\begin{aligned}(\eta', \eta_t)_{g(\eta)} &= \sum_n \int_{\Omega_n} (\Theta_n)_t\,\Theta'\,\mathrm{d}x \\ &= \sum_n \int_{\Gamma_n^+} (\Theta_n)_t\,\Theta'|\ell|\mathrm{d}\gamma.\end{aligned} \tag{100}$$

Here each boundary $\partial\Omega_n$ is subdivided into two curves Γ_n^+ and Γ_n^- so that if $x(s) \in \Gamma_n^+$, the conjugate point $\tilde{x}(s) \in \Gamma_n^-$ and $\Theta(x) < \Theta(\tilde{x})$. Using the Frenet formula $\mathrm{d}\hat{\mathbf{t}}/\mathrm{d}s = -\kappa\hat{\mathbf{n}}$ and comparing (93) and (94) with (51), it follows that

$$\begin{aligned}(\eta', \eta_t)_{g(\eta)} &= \frac{1}{2}\sum_n \int_{\Gamma_n^+} \left(-\left(\frac{G^{-1}R_s}{\sqrt{1-\Phi_s^2}} \right)_{x(s)}^{\tilde{x}(s)} + \left[\frac{G^{-1}\mathbf{T}_s \cdot \hat{\mathbf{n}}}{1-\Phi_s^2} \right]_{x(s)}^{\tilde{x}(s)} \right) \Theta_n' \mathrm{d}\gamma \\ &= \frac{1}{2}\sum_n \int_{\Gamma_n^+} \left(-\frac{R_s}{\sqrt{1-\Phi_s^2}} - \frac{\sigma \mathbf{T}_s \cdot \hat{\mathbf{n}}}{1-\Phi_s^2} \right) \Theta_n' G^{-1} \mathrm{d}\gamma + \frac{1}{2}\sum_n \int_{\Gamma_n^-} \left(-\frac{R_s}{\sqrt{1-\Phi_s^2}} + \frac{\sigma \mathbf{T}_s \cdot \hat{\mathbf{n}}}{1-\Phi_s^2} \right) \Theta_n' G^{-1} \mathrm{d}\gamma. \end{aligned} \tag{101}$$

Using (74) and (90) allows this to be written as

$$(\eta', \eta_t)_{g(\eta)} = \frac{1}{2}\sum_n \int_{\partial\Omega_n} \left(-R_s + \frac{\sigma \mathbf{T}_s \cdot \hat{\mathbf{n}}}{\sqrt{1-\Phi_s^2}} \right) \left(\Phi' - \sigma\sqrt{1-\Phi_s^2}(\mathbf{x}' \cdot \hat{\mathbf{n}}) + \Phi_s(\mathbf{x}' \cdot \hat{\mathbf{t}}) \right) \mathrm{d}s. \tag{102}$$

The sum over boundaries of each grain can be rewritten as a sum over each curve Γ_i. Note that because $\hat{\mathbf{n}}$ is defined relative to each grain, this implies cancellation of cross-terms that involve the normal exactly once when summing over all grains. It is simple to show that $R_s\,\Phi_s = -\mathbf{T}_s \cdot \hat{\mathbf{t}}$, which means that, by writing $\mathbf{x}' = (\mathbf{x}' \cdot \hat{\mathbf{n}})\hat{\mathbf{n}} + (\mathbf{x}' \cdot \hat{\mathbf{t}})\hat{\mathbf{t}}$,

$$(\eta', \eta_t)_{g(\eta)} = -\sum_i \int_{\Gamma_i} R_s\,\Phi' + \mathbf{T}_s \cdot \mathbf{x}'\,\mathrm{d}s = -\langle \delta E, \eta' \rangle \tag{103}$$

which demonstrates (99).

6. Conclusions

The main result of this paper is to demonstrate that a free boundary problem for grain boundary curves arises as the limiting dynamics of (1). As with all formal asymptotic analysis, the conditions derived should be regarded as necessary but not sufficient for the expansion to succeed. The variational character of the reduced problem, however, provides some reassurance about the formal calculation.

A likely advantage to the sharp interface dynamics is for large scale numerical computation. There are many similarities between our problem and that of curvature-driven crystalline grain boundary network dynamics, for which numerical algorithms have been developed [3]. Some additional challenges would need to be overcome, in particular tracking the motion of characteristic curves which connect points on adjacent grain boundaries. A different strategy would be to utilize asymptotic information to ameliorate numerical stiffness and grid resolution problems in the original partial differential equation (e.g. [11]).

Work is needed to fully understand the stability and evolution of grain boundary junctions. Stability is likely a function of both energetics and topology. For example, a quadruple extrema junction cannot break into two triple junctions; a saddle would also have to be created. It is also interesting to note that junction and grain boundary nucleation can arise rather naturally, because junctions are really just critical points of the ambient function Θ.

This paper will hopefully provide groundwork for many other problems. Among them are gradient evolutions with anisotropic energies, e.g.

$$E = \int \frac{\epsilon}{2}(\Delta\Theta)^2 + W(\nabla\Theta)\mathrm{d}x \tag{104}$$

where W has minima at the vertices of a regular polygon. Other incarnations of phase diffusion equations may also be treatable by the expansion procedure outlined, even when they do not possess a variational character. A more ambitious achievement would be to incorporate descriptions of disclinations and other one dimensional defects together with grain boundary dynamics.

Acknowledgments

The author has benefited from discussions with Alan Newell. This work was partially supported under NSF award DMS-0405596.

References

[1] L. Ambrosio, C. De Lellis, C. Mantegazza, Line energies for gradient vector fields in the plane, Calc. Var. Partial Differential Equations 9 (1999) 327–355.
[2] P. Aviles, Y. Giga, The distance function and defect energy, Proc. Roy. Soc. Edinburgh Sect. A 126 (1996) 923–938.
[3] L. Bronsard, B.T.R. Wetton, A numerical method for tracking curve networks moving with curvature motion, J. Comput. Phys. 120 (1995) 66–87.
[4] G. Caginalp, P. Fife, Dynamics of layered interfaces arising from phase boundaries, SIAM J. Appl. Math. 48 (1988) 506–518.
[5] M.C. Cross, A.C. Newell, Convection patterns in large aspect ratio systems, Physica D 10 (1984) 299–328.

[6] A. DeSimone, S. Müller, R.V. Kohn, F. Otto, A compactness result in the gradient theory of phase transitions, Proc. Roy. Soc. Edinburgh Sect. A 131 (2001) 833–844.
[7] N.M. Ercolani, R. Indik, A.C. Newell, T. Passot, The geometry of the phase diffusion equation, J. Nonlinear Sci. 10 (2000) 223–274.
[8] D.J. Eyre, Unconditionally gradient stable time marching the Cahn-Hilliard equation, in: Computational and mathematical models of microstructural evolution, (San Francisco, CA, 1998), in: Mater. Res. Soc. Sympos. Proc., vol. 529, MRS, Warrendale, PA, 1998, pp. 39–46.
[9] P. Fratzl, J.L. Lebowitz, Universality of scaled structure functions in quenched systems undergoing phase separation, Acta Metall. 37 (1989) 4794–4811.
[10] H. Garcke, B. Nestler, B. Stoth, On anisotropic order parameter models for multi-phase systems and their sharp interface limits, Physica D 115 (1998) 87–108.
[11] K. Glasner, Nonlinear preconditioning for diffuse interfaces, J. Comput. Phys. 174 (2001) 695–711.
[12] K. Glasner, A diffuse interface approach to Hele–Shaw flow, Nonlinearity 16 (2003) 1–18.
[13] K. Glasner, T. Witelski, Coarsening dynamics of dewetting films, Phys. Rev. E 67 (2003) 016302.
[14] A. Hubert, R. Schafer, Magnetic Domains, Springer, 1998.
[15] D. Kinderlehrer, C. Liu, Evolution of grain boundaries, Math. Models Methods Appl. Sci. 11 (2001) 713–729.
[16] R.V. Kohn, F. Otto, Upper bounds on coarsening rates, Comm. Math. Phys. 229 (2002) 375–395.
[17] R.V. Kohn, X. Yan, Upper bound on the coarsening rate for an epitaxial growth model, Comm. Pure Appl. Math. 56 (2003) 1549–1564.
[18] I.M. Lifshitz, V.V. Slyozov, The kinetics of precipitation from supersaturated solid solutions, J. Chem. Phys. Solids 19 (1961) 35–50.
[19] D. Moldovan, L. Golubovic, Interfacial coarsening dynamics in epitaxial growth with slope selection, Phys. Rev. E (Statistical Physics, Plasmas, Fluids, and Related Interdisciplinary Topics) 61 (2000) 6190–6214.
[20] A.C. Newell, T. Passot, C. Bowman, N. Ercolani, R. Indik, Defects are weak and self-dual solutions of the cross-newell phase diffusion equation for natural patterns, Physica D 97 (1996) 185–205.
[21] M. Ortiz, G. Gioia, The morphology and folding patterns of buckling-driven thin-film blisters, J. Mech. Phys. Solids 42 (1994) 531–559.
[22] M. Ortiz, E.A. Repetto, H. Si, A continuum model of kinetic roughening and coarsening in thin films, J. Mech. Phys. Solids 47 (1999) 697–730.
[23] F. Otto, Dynamics of labyrinthine pattern formation in magnetic fluids: A mean-field theory, Arch. Ration. Mech. Anal. 141 (1998) 63–103.
[24] R.L. Pego, Front migration in the nonlinear Cahn-Hilliard equation, Proc. R. Soc. Lond. A 422 (1989) 261–278.
[25] M. Rost, J. Krug, Coarsening of surface structures in unstable epitaxial growth, Phys. Rev. E (Statistical Physics, Plasmas, Fluids, and Related Interdisciplinary Topics) 55 (1997) 3952–3957.
[26] M. Siegert, M. Plischke, Slope selection and coarsening in molecular beam epitaxy, Phys. Rev. Lett. 73 (1994) 1517–1520.
[27] A.A. Wheeler, G.B. McFadden, A ξ-vector formulation of anisotropic phase-field models: 3d asymptotics, European J. Appl. Math. 7 (1996) 367–381.